Modeling Water Vapor Transport at Liquid/Membrane Interfaces for Applications in Liquid Desiccant Air Conditioners

Cooperative Research and Development Final Report

CRADA Number: CRD-17-679

NREL Technical Contact: Jason Woods

NREL is a national laboratory of the U.S. Department of Energy
Office of Energy Efficiency & Renewable Energy
Operated by the Alliance for Sustainable Energy, LLC

This report is available at no cost from the National Renewable Energy Laboratory (NREL) at www.nrel.gov/publications.

Contract No. DE-AC36-08GO28308

Technical Report
NREL/TP-5500-77201
July 2020

Modeling Water Vapor Transport at Liquid/Membrane Interfaces for Applications in Liquid Desiccant Air Conditioners

Cooperative Research and Development Final Report

CRADA Number: CRD-17-679

NREL Technical Contact: Jason Woods

Suggested Citation
Woods, Jason. 2020. *Modeling Water Vapor Transport at Liquid/Membrane Interfaces for Applications in Liquid Desiccant Air Conditioners: Cooperative Research and Development Final Report, CRADA Number CRD-17-679.* Golden, CO: National Renewable Energy Laboratory. NREL/TP-5500-77201. https://www.nrel.gov/docs/fy20osti/77201.pdf.

NREL is a national laboratory of the U.S. Department of Energy
Office of Energy Efficiency & Renewable Energy
Operated by the Alliance for Sustainable Energy, LLC

This report is available at no cost from the National Renewable Energy Laboratory (NREL) at www.nrel.gov/publications.

Contract No. DE-AC36-08GO28308

Technical Report
NREL/TP-5500-77201
July 2020

National Renewable Energy Laboratory
15013 Denver West Parkway
Golden, CO 80401
303-275-3000 • www.nrel.gov

NOTICE

This work was authored by the National Renewable Energy Laboratory, operated by Alliance for Sustainable Energy, LLC, for the U.S. Department of Energy (DOE) under Contract No. DE-AC36-08GO28308. Funding provided by U.S. Department of Energy Office of Energy Efficiency and Renewable Energy Advanced Manufacturing Office. The views expressed herein do not necessarily represent the views of the DOE or the U.S. Government.

This report is available at no cost from the National Renewable Energy Laboratory (NREL) at www.nrel.gov/publications.

U.S. Department of Energy (DOE) reports produced after 1991 and a growing number of pre-1991 documents are available free via www.OSTI.gov.

Cover Photos by Dennis Schroeder: (clockwise, left to right) NREL 51934, NREL 45897, NREL 42160, NREL 45891, NREL 48097, NREL 46526.

NREL prints on paper that contains recycled content.

Cooperative Research and Development Final Report

Report Date: June 30, 2020

In accordance with requirements set forth in the terms of the CRADA agreement, this document is the final CRADA report, including a list of subject inventions, to be forwarded to the DOE Office of Scientific and Technical Information as part of the commitment to the public to demonstrate results of federally funded research.

Parties to the Agreement: 7AC Technologies

CRADA Number: CRD-17-679

CRADA Title: Modeling Water Vapor Transport at Liquid/Membrane Interfaces for Applications in Liquid Desiccant Air Conditioners

Joint Work Statement Funding Table showing DOE commitment:

Estimated Costs	NREL Shared Resources a/k/a Government In-Kind
Year 1	$300,000.00
TOTALS	$300,000.00

Abstract of CRADA Work:

Conventional compressor-based cooling has undergone incremental changes over the past 100 years. Further improvements in efficiency require evermore complex systems, especially under humid conditions. Meso-porous membranes offer unique opportunities for efficient humidity control in buildings using an absorbent desiccant solution, but membranes are not designed or optimized for this purpose. This project will use molecular dynamic simulations to determine optimal membrane properties for these air conditioning applications, focusing on the membrane properties at the membrane/liquid/air interface. Optimal membrane designs will enable smaller, more durable, and less expensive designs of these membrane air conditioning systems.

Summary of Research Results:

This section describes the completed work and outcomes of this project, including slight changes to the original joint work statement (JWS). The work completed for each task of the JWS is described under the headings below, while conclusions and outcomes from the work are summarized in a separate section at the end.

This section starts with background and an explanation of the modeling approach.

Introduction & motivation:
Conventional compressor-based cooling has undergone incremental changes over the past 100 years. Further improvements in efficiency require evermore complex systems, especially under

humid conditions. 7AC Technologies has developed an approach to liquid desiccant air conditioning which has demonstrated improved thermodynamic performance, when coupled with traditional compressor-based HVAC systems.

These porous membranes offer unique opportunities for efficient humidity control in buildings using an absorbent desiccant solution, but membranes are not designed or optimized for this purpose.

This project originated from a request from 7AC Technologies, who was interested in better understanding the physics occurring at the membrane/desiccant/air interface. They requested molecular dynamics simulation support to help understand this interface better and determine better membrane properties for their application. 12

This project used molecular dynamic (MD) simulations to determine the effect of membrane properties on important metrics for these air-conditioning applications, focusing on the membrane properties at the membrane/liquid/air interface. Using improved membranes will enable smaller, more durable, and less expensive designs of these membrane air conditioning systems.

Problem description:
7AC's interests align with the two key performance indicators of any liquid-to-air membrane contactor: breakthrough pressure, and vapor transport through the membrane pores. They are also interested in preventing crystallization of salt hydrates out of the desiccant solution.

Breakthrough pressure:
In these membrane contactor applications, liquid enters the pores, sometimes referred to as pore breakthrough or pore wetting, when the force from the liquid pressure exceeds the surface tension forces. This *breakthrough pressure* depends on the membrane material and the pore size, as predicted by the Young-Laplace equation. For aqueous applications, the membrane material is hydrophobic, with a low surface energy (e.g., polypropylene, PTFE). The breakthrough pressure is also inversely proportional to pore size. The effect of pore shape is less understood, with many researchers using an empirical coefficient to consider the deviation from cylindrical pores. A model for breakthrough pressure of torus-shaped pores, representative of fibrous membranes, was also developed by Purcell [1], and has been used by several membrane researchers.

Because of the importance of pore morphology on pore breakthrough, it is important to understand how it influences breakthrough pressure.

The breakthrough of liquids into hydrophobic membranes is governed by the Young-Laplace equation:

$$\Delta p = \gamma \left(\frac{1}{R_{curv,1}} + \frac{1}{R_{curv,2}} \right) \quad (1)$$

where Δp is the breakthrough pressure, γ the liquid surface tension, and $R_{curv,1}$ and $R_{curv,2}$ the two principal radii of curvature of the liquid/gas interface (Figure 1).

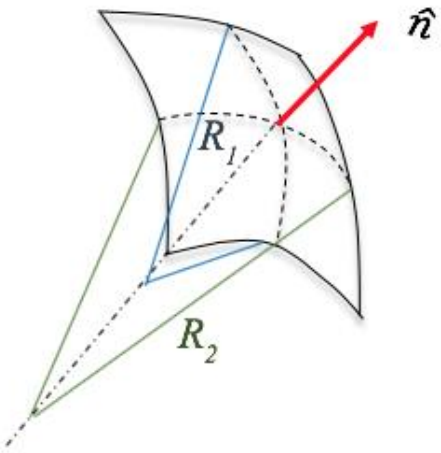

Figure 1: Curved liquid interface showing the two principal radii of curvature.

This equation governs not only liquid entry into a membrane pore, but also capillary rise, the pressure inside water droplets in air, and the pressure of gas bubbles in water. This equation can be put into more familiar terms for membrane researchers by calculating the radii of curvature for a straight-through, cylindrical pore with sharp edges. Then this equation becomes:

$$\Delta p = \frac{-2\gamma cos\theta}{r_{pore}} \tag{2}$$

where r_{pore} is the membrane pore radius, and theta is the contact angle (Fig. 1). A pore morphology, or pore geometry, coefficient (*B*) can be added to account for the effect of non-cylindrical pores:

$$\Delta p = \frac{-2B\gamma cos\theta}{r_{pore}} \tag{3}$$

This was first introduced by Cotton [2] in 1981 for mercury porosimetry, and has been used extensively since to model pore breakthrough.

While some have argued that the Young-Laplace equation does not predict breakthrough pressure well, this is misleading because they are arguing that Eq. (2) or Eq. (3) does not predict breakthrough pressure well, but Eq. (1) is the Young-Laplace equation, which is still valid for any pore size and shape.

Other models specific to different geometries have also been developed. For example, several membrane researchers [3-8] have used an equation valid for torus-shaped pores, originally developed by Purcell [1] for capillary flow through porous subsurface rocky soils:

where R_{fiber} is the radius of the torus cross section (formed by a hypothetical polymer fiber), and α is the angular distance the liquid-gas interface progresses past the torus midline (Fig. 2). This angle can be calculated with:

$$\sin(\theta + \alpha) = \frac{sin\theta}{1 + \frac{r_{pore}}{R_{fiber}}} \tag{4}$$

This model is still based on a circular cross-section but includes the effect of axial variation in pore geometry, similar to a membrane with cylindrical fibers forming these torus-shaped pores. This model is still based on the original Young-Laplace equation, Eq. (1), but the radii of curvature change as the liquid/gas contact line moves axially within the pore. Eq (2) matches Eq. (4) when $\alpha = 0$ ($r_{pore} << R_{fiber}$).

Thus, the only equation in the literature for calculating the impact of pore cross-sectional shape is the *B* coefficient in Eq. (3), which is used extensively in the literature. However, only a few papers have tried to link the actual pore geometry to the B coefficient, all of which have been empirical, and thus likely has *B* and α lumped into one coefficient.

One final equation, suggested by Hereijgers et al. [7] is to include an empirical coefficient to account for the effect of both cross sectional and axial shape:

$$\Delta p = \frac{-2B_0\gamma\cos(\theta + \alpha_0)}{r_{pore}} \quad (5)$$

In general, β_0 is different than B. This equation can be thought of as a generalized equation for pore breakthrough, whose parameters can be investigated with molecular dynamic simulations.

Evaporation/condensation rates:
Evaporation and condensation occur at the liquid/vapor interface, and are key drivers in the total vapor transport through the membrane. 7AC Technologies is very interested in understanding how membrane pores can impact evaporation or condensation of water vapor from the liquid desiccant. Specifically, they want to know if there are any nanoscale effects that impact condensation and evaporation processes differently. They have some experimental evidence that evaporation is a lower rate than expected in their membrane modules, although there are many other factors that could be contributing to this phenomenon. Part of the motivation of this project is to determine if there are any microscopic effects that could contribute to this phenomenon, or if it is likely from some other cause.

Prior to, and in parallel with, performing the molecular dynamics simulations, National Renewable Energy Laboratory (NREL) also modeled the desiccant absorption and desorption process for the design developed by 7AC. This included gas-diffusion-theory calculations for transport of water vapor through the pores, and a finite-difference model of the water, air and desiccant in their membrane module. The finite-difference model showed that regeneration of the desiccant (i.e., evaporation) is much more sensitive to non-idealities in their process than the absorption process (i.e., condensation). The non-infinite flow rates and non-zero temperature and concentration gradients causes these non-idealities, and the performance of the regeneration process is much more sensitive than the absorption process [9].

Even with these known differences between the regeneration and absorption processes, the regeneration / evaporation process still showed lower performance than the model predicts, whereas the absorption / condensation process was more in-line with the model predictions. Based on standard mass transfer and diffusion calculations, including the non-zero velocity of airflow through the pores in the 7AC design, the difference between the evaporation and condensation rates were the same for the same driving potential. This motivated the molecular dynamics simulations to better understand how the membrane may impact evaporation or condensation.

Crystallization:
The final area of interest to 7AC is the crystallization of the desiccant, which can damage the membrane module, or prevent it from operating. This is often referred to as inorganic fouling or scaling in the membrane distillation field (a process similar to the process used by 7AC). Crystallization is caused when the concentration of salt ions exceeds the solubility limit of the desiccant ions. Part of this research investigated the potential for crystallization at the membrane surface (i.e., heterogeneous nucleation) versus crystallization in the bulk liquid (i.e., homogenous nucleation).

Task 1: Model development for desiccant, air, membrane interface
Our approach focused on molecular dynamic (MD) simulations of the interactions between water/desiccant solutions with polymer membranes. In general, we used Amber molecular dynamics packages to perform simulations with a time step of 2 fs and periodic boundary conditions. The polypropylene (PP) (010) surface (Figure 2A) was adapted from PP crystalline structure, in which the parallel PP fiber forms a smooth surface. The PP fibers were fixed during simulations to retain this smoothness. The force field parameters for atoms were from established OPLS-AA force field for the membrane and the widely-used TIP3P water model. Long-range electrostatics (charge-charge) interaction was treated with particle mesh Ewald summation using mesh density of ~ 1 point/Å in each cell direction. The system was first equilibrated at targeted temperature. Calculations were performed on the NREL's Peregrine high-performance computer system.

Contact angle:
In the contact angle simulations, a water (or desiccant) droplet with a diameter of 5nm was put on a PP surface at 298K (Figure 2). We ran one simulation for 6ns and then calculated the average profile of the droplet using the simulation trajectory. The calculated profile curve was then fitted to a circle to obtain the contact angle at the PP surface.

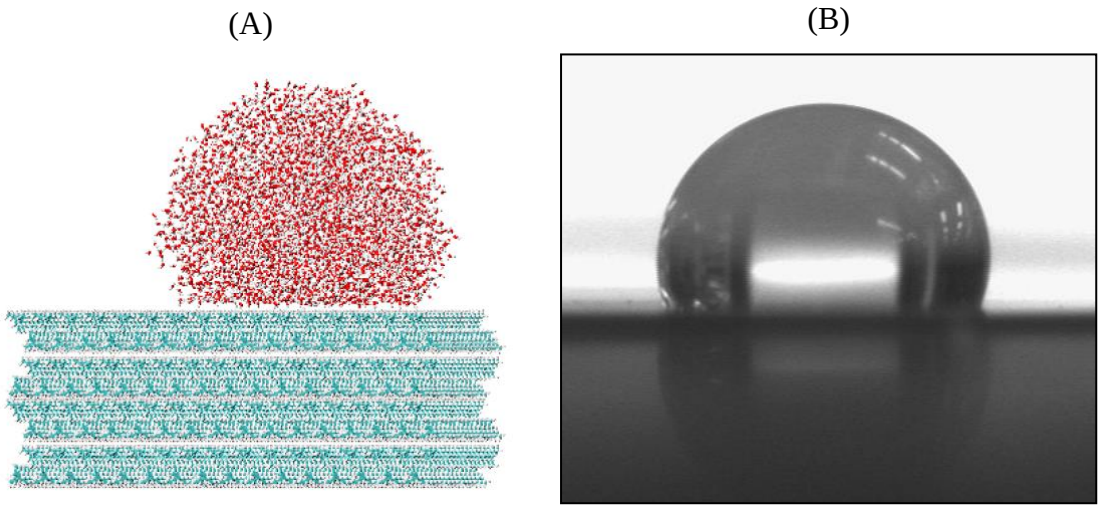

Figure 2. (A) A snapshot from MD simulation: One 5 nm water droplet on the PP membrane (010) surface. (B) Experimental measurement for the contact angle.

Task 2: Evaporation/condensation rates:
We designed a steady state simulation of evaporation process by moving evaporated water molecule from the gas phase and putting them back to the liquid phase. Figure 3A illustrates such a system for evaporation and a similar method can be used to create a steady state of condensation by moving water molecules form liquid phase to the gas phase. We also created transient state simulations by suddenly change the RH to 120% or 80% and measure the speed for the system goes back to the equilibrium (Figure 4A).

Task 4: Breakthrough pressure
To simulate a breakthrough process, we applied an external force on every water molecule to force it passing through a slit or pore formed by parallel PP fibers. We run simulations at many different pressure parallelly and the lowest pressure to make the water breaking through the slit/pore is defined as the breakthrough pressure. We found that the breakthrough time is depend on the size of the slit/pore and the thickness of the membrane and generally are between 2ns and 20ns. We have made sure that our simulation time is long enough to make a breakthrough to occur.

Task 4: Crystallization:
MD simulations were performed at 298K on the system of Figure 8A and the trajectory was used to generate maps of Li^+ and Cl^- concentrations by calculating number of ions inside each grid bin. The simulation of formation of LiCl crystal was performed by removing water molecules in the gas phase at 600K. In this way, we created a chemical potential bias to prevent the system from reaching equilibrium, and this continuous evaporation leads to crystallization of LiCl salt.

Task 2: Simulations for Evaporation/Condensation on the desiccant/air interface
In this section, we focus on the evaporation and condensation process and the influence of the pores. We first focused on the equilibration property and tried to calculate the vapor pressure of desiccant at different concentration using three different method: direct simulation, umbrella sampling, and thermodynamic integration.

The first method is to directly measure the vapor pressure by calculating the concentration of water in the gas phase above the liquid desiccant phase. This approach resulted in a linear relationship with the concentration of desiccant, which is not consistent with the non-linear relationship of experimental measurement. We then used umbrella sampling method, in which one water molecule was gradually pulled up from the liquid phase to the gas phase by an external force. By measuring the force applied during the simulation, we can calculate the free energy used to evaporate one water molecule, and then the vapor pressure. However, pulling different water molecules results in dramatically different results, leading to unacceptable uncertainty. The third method is thermodynamic integration, where we artificially removed a water molecule from the liquid phase and then artificially added it to the gas phase. Again, the change in free energy was measured, and used to calculate vapor pressure. However, our result shows little change in the free energy when desiccant concentration is increasing. As a result, we didn't find any effective method to calculate the vapor pressure of the desiccant.

We then investigated the kinetics of evaporation and condensation by simulating evaporation and condensation from liquid/vapor interfaces, including with membrane pores. We used two different methods: a steady-state simulation method, and a transient method.

Steady-state evaporation/condensation: Figure 3B shows the normalized evaporation rate at 500K as a function of humidity bias to the equilibration in relative humidity (RH). These results are based on the simulation setup shown in Figure 3A, where the driving force was maintained constant by removing ions from the vapor above the membrane. The results indicate that pore size has little impact on the evaporation/condensation rates. The condensation rate is always larger than the evaporation rate at the same humidity bias (driving force). To investigate this further, we also used a transient simulation method, where the concentration of vapor above the liquid slowly changed towards equilibrium.

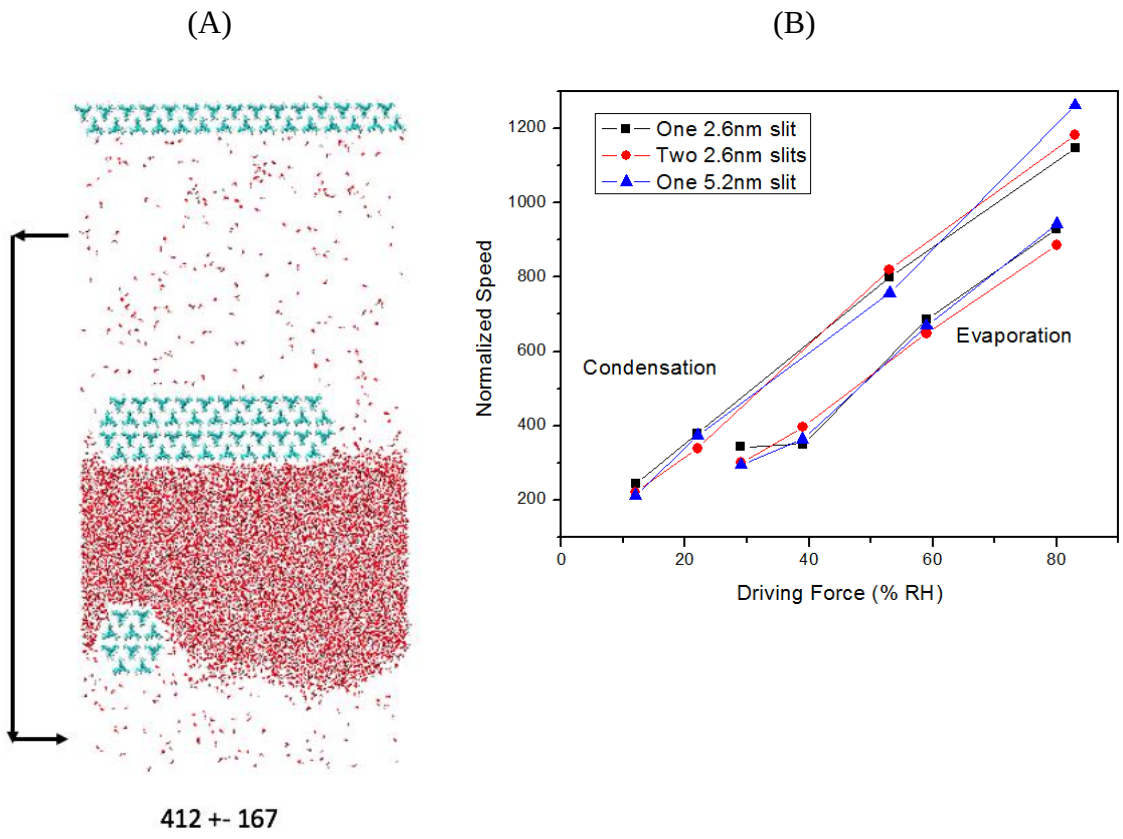

Figure 3. (A) Steady state simulation of evaporation process and (B) evaporation/condensation rate as a function of driving force.

Transient evaporation/condensation simulations:
In these transient simulations, the humidity above liquid water started either 20% above or below the saturation vapor pressure, to simulate evaporation from the liquid (vapor below saturation) or condensation (vapor above saturation). We ran these simulations both with only water vapor in the space above the liquid, and with N_2 molecules (N_2: H_2O ratio is 7:1).

Both sets of simulations showed similar results. Figure 4 shows the results of the transient simulations with no N_2, with Figure 4B showing the number of water molecules in the region between 7.5nm and 20.0nm. The number of water molecules in the vapor phase decreases during condensation and increases during evaporation. Figure 4C takes an average of the two curves in Figure 4B and calculates the difference, which shows that the average values were smaller than

the equilibration value for most of time, confirming that the overall condensation rate is faster than the evaporation rate. However, we also made these same average plots for two sub-regions: 7.5-12nm (Figure 4D) and 12-20nm (Figure 4E). The plot for the 7.5-12nm shows that this region is closer to the equilibration values. This suggests that in the region close to the liquid water, condensation and evaporation rates are roughly equal. In other words, the rate of water molecule transport from the 12-20nm region, and to the 7.5-12nm region, is higher during condensation. But that these molecules move from the 7.5-12nm region into the liquid water (or vice versa during condensation) at roughly the same speed regardless of direction.

A final simulation introduced the membrane (with a pore) above the gas-liquid phase (similar to the slit in Figure 3A). The transient simulations were again started with water vapor either 20% above or below the saturation vapor pressure. The results aligned with the case without a membrane: the condensation and evaporation rates in the region near the liquid/vapor interface are nearly the same, but the diffusion rates further from the interface were higher for condensation than for evaporation. This implies that although the actual rate of liquid-vapor phase change at the liquid/vapor interface is the same, regardless of whether it is evaporation or condensation, the water molecule diffusion in the regions far from the interface plays an important role in determining the overall condensation and evaporation rates.

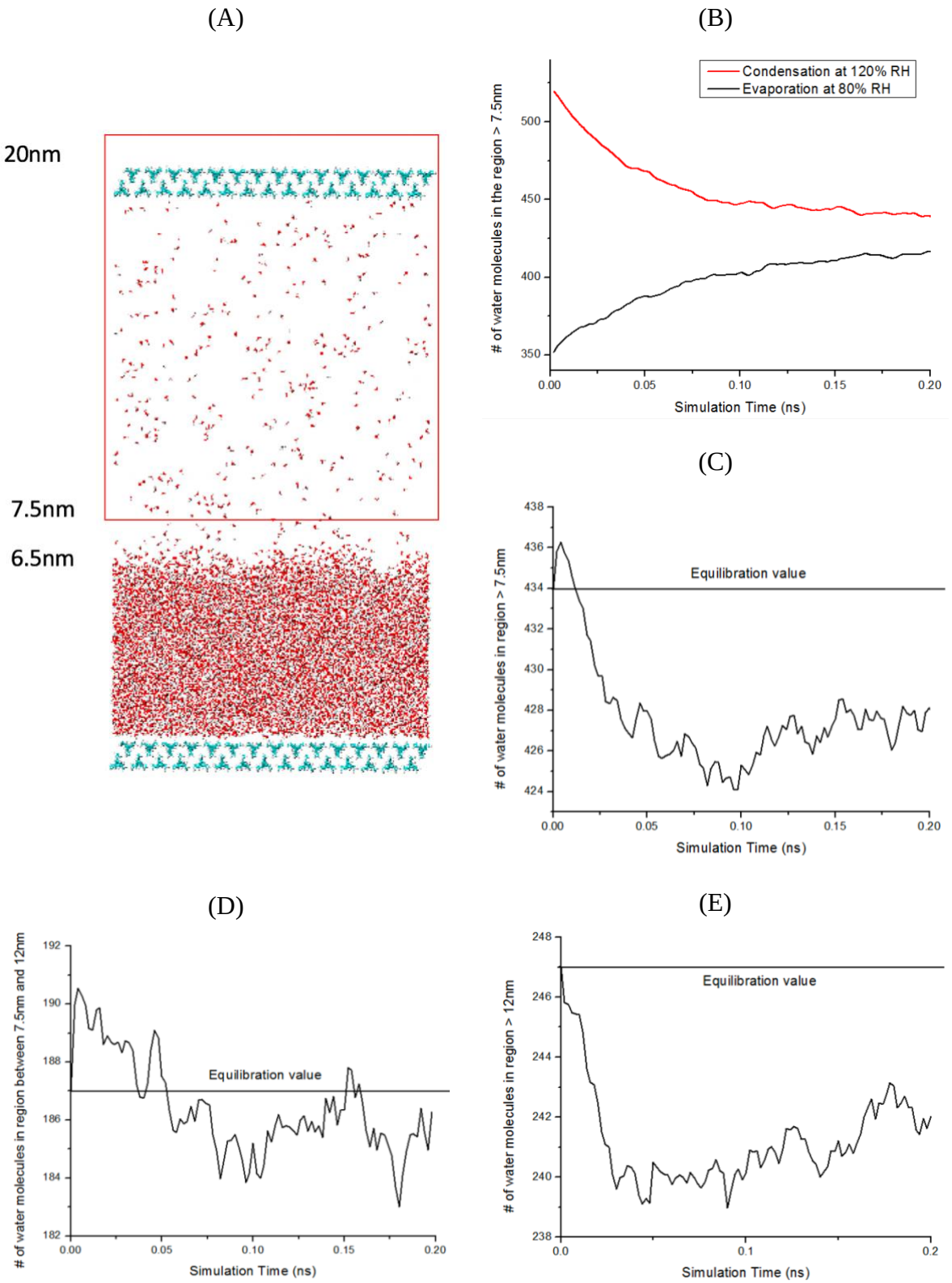

Figure 4. (A) Transient state simulation system; (B) Condensation and evaporation plots as a function of simulation time; (C) The average plot of condensation and evaporation; (D) The average plots for regions between 7.5-12nm and (E) 12-20nm.

Task 3: Simulations for vapor transport through membrane pores

During the project, it was decided to stay focused on the membrane/liquid interface, including how it impacts evaporation and condensation, as well as breakthrough pressure through the membrane pores. While we did explore some methods for modeling this vapor transport, this task was omitted from this current project.

Task 4: Simulations for the desiccant/membrane/air interface

Contact Angle:
Since this project focuses on the interactions between the membrane and desiccant solution, it's important to choose parameters with accurate descriptions of the surface tension. When we started this project, there were multiple sets of MD force fields available for the membrane, desiccant (LiCl), and water. In order to identify the optimal force field parameters, we have run tens of simulations to study contact angles of pure water and desiccant on the polypropylene (PP) with different force field parameters and compared with experimental measurements. The contact angles determined by MD simulations on the (010) PP surface are 115° for pure water and 126° for 30% LiCl using TIP3P water model. For SPC water model, they are 118° and 127°, respectively. Our experimental measurements of contact angles for pure water and 30% LiCl on PP membrane are 108° and 114°, respectively. Thus, TIP3P water model results are closer to the experimental measurement and we used this model in the following simulations.

Breakthrough pressure:
We then focused on the breakthrough phenomenon at the liquid/membrane interfaces, as the most important function of the membrane used in liquid desiccant air conditioners is to prevent liquid from breaking through. The Young-Laplace equation describes the relationship between the breakthrough pressure Δp and the curvature of the pores, as discussed in the *problem description.*

When the pore is a circle, $R_1=R_2=r/\cos\theta$, where r is the radius of the pore. For an infinite long slit, $R_1= d/\cos\theta$ and $R_2=\infty$, where d is the width of the slit. However, for non-axisymmetric pores, there is no universal relationship between the R_1/R_2 and pore's size. The results presented here can be used to generalize the results to different pore shapes.

Figure 5 shows the five different slit shapes that have the same minimum gap width (*d*). The thickness of PP slab is 4nm. We found that for the same shape, breakthrough pressure has a linear relationship with *1/d* (Figure 7). The ratios between intercept and slope are all < 1%. This is consistent with the Young-Laplace equation where breakthrough pressure $\Delta p=\gamma\cos\theta/d$. However, the converging gap shape (10000) has the lowest slope, *i.e.* the lowest breakthrough pressure, and its breakthrough pressure is only ~80% of diverging gap shape (00001). This result indicate that the breakthrough pressure not only depends on the gap size of a slit, but also depends on the cross-section. This is consistent with the effect of the angle α from the Purcell model mentioned above [1].

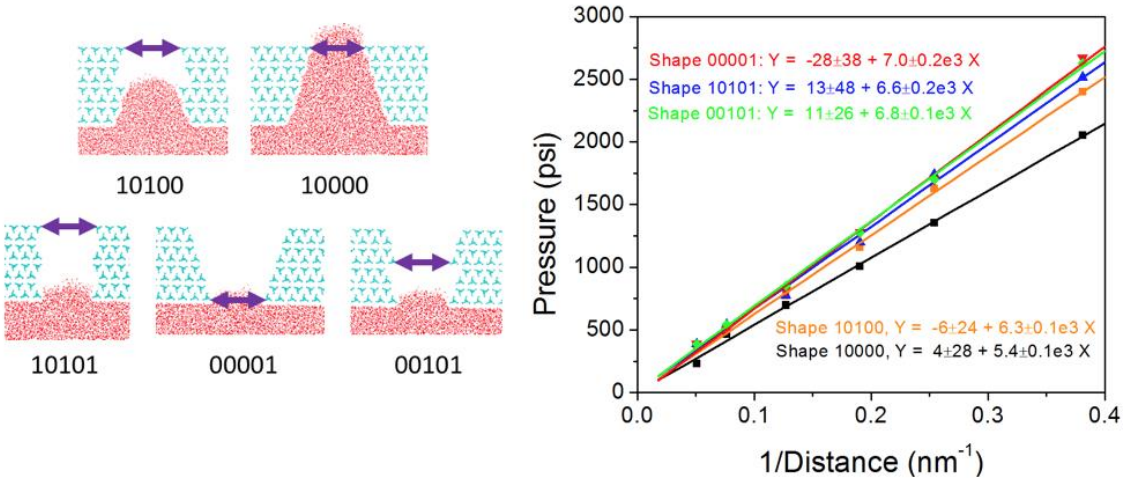

Figure 5. Break-though pressure for 'slit' pores with different through-pore shapes

We also performed MD simulations on different pore cross-sectional shapes and measured breakthrough pressures (Figure 6). The breakthrough pressure is still proportional to *1/a* with different slopes for different shapes, where *a* is the size of the pore. We defined an effective *d*. A circle with this *d* will have the same area of a certain shape. For example, for a square shape pore with length of *a*, its area is: $S = a^2 = \pi d^2/4$, so $d = 2a/\sqrt{\pi}$. By plotting the breaking through pressure as a function of *1/d* (Figure 7), we have found that the slopes become very similar for different shapes. The largest slope is 112% of the smallest slope. This is useful to estimate breakthrough pressure for pores with different shapes with an error < 15%.

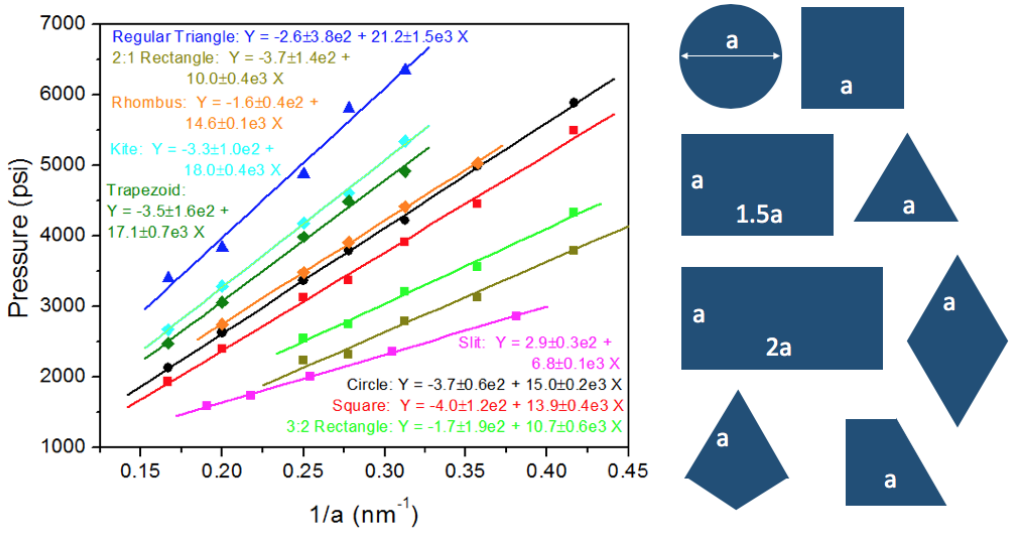

Figure 6. Breaking though pressure for different shapes of pores.

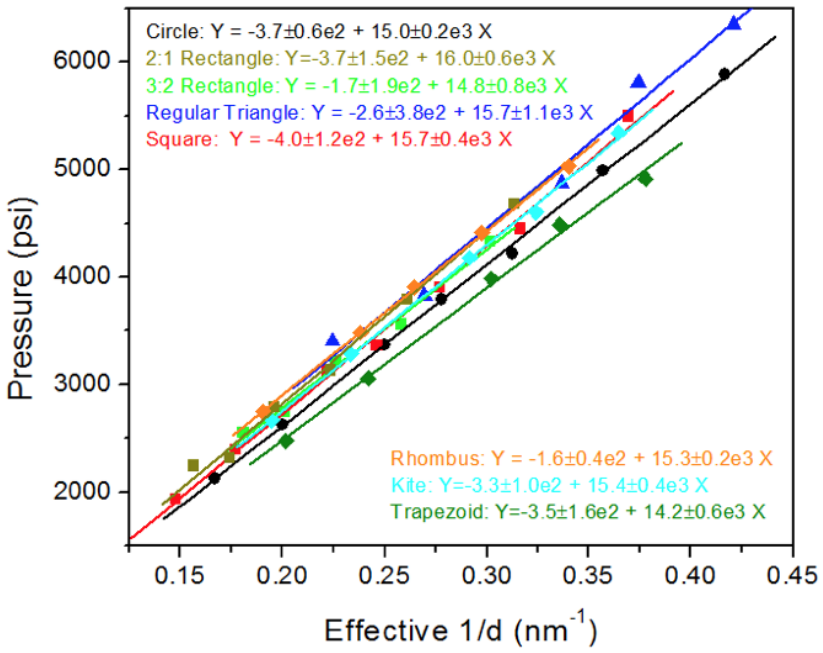

Figure 7. Breaking though pressure as a function of 1/d.

Use MD simulations to investigate the ion distribution in LiCl interface to investigate its equilibrium property at 298K. Figure 8B is the net charge map calculated by $[Li^+] - [Cl^-]$. The water/air interface shows a light-orange color, indicating a positively charged interface. The water/PP interface has showing discontinuous yellow colors, indicating that the Li^+ is closer to the PP surface than the Cl^-.. Considering that both experimental and computational measurements show the diffusion rate coefficient of Li^+ is smaller than Cl^-'s, the higher concentration of Li^+ and slow diffusion rate imply that Li^+ plays an more important role in crystallization than Cl^-.

Crystallization of lithium chloride salt or hydrates at the membrane surface:
We also simulated the crystallization of LiCl by removing water molecules in the gas phase at 600K. After 24ns, we observed the formation of highly ordered LiCl crystal (Figure 9A). However, there is still ~4% water molecules left, mainly locating between the salt crystal and the membrane. This implies that the water-PP interaction is preferred instead of the LiCl-PP interaction. Thus, the membrane itself is not a good candidate for the crystallization site and the crystallization may arise from the local ion concentration fluctuations in the bulk solution as shown in Figure 8B or charged foulants on the surface. This means that clean membranes should resist crystallization better than membranes that have fouling from contaminants in the air or liquid streams.

(A) (B)

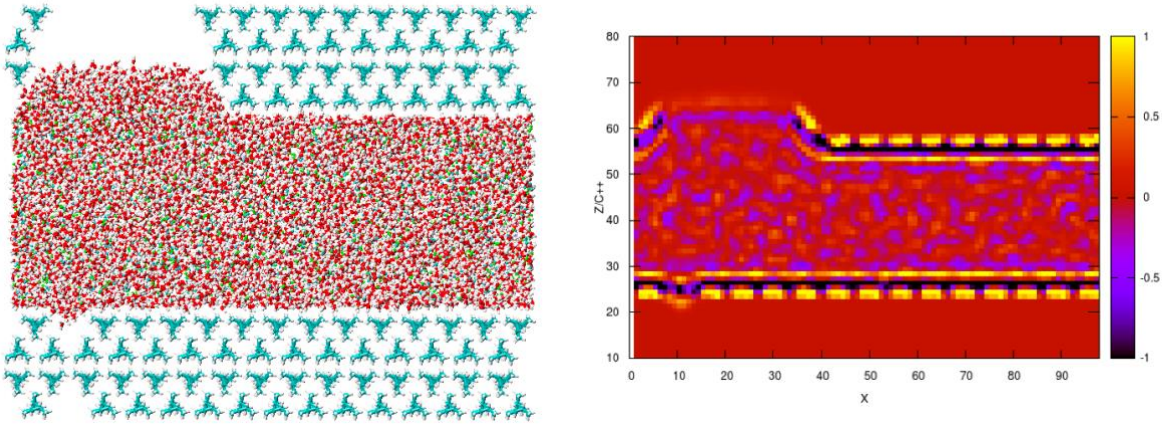

Figure 8. (A) 30% LiCl in a gap formed by PP membranes and (B) net charge maps.

(A) (B)

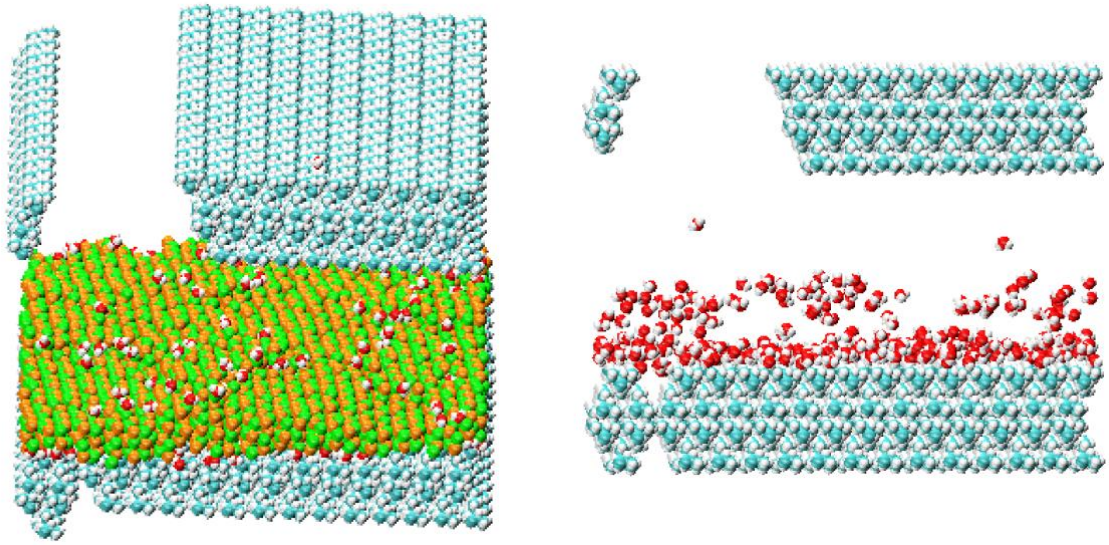

Figure 9. (A) Crystal formed after the simulation and (B) remaining water molecules without showing LiCl crystal.

Task 5: Publications and reporting

Under this task, we provided quarterly progress reports to the primary sponsor (US DOE Advanced Manufacturing Office, AMO), as well as a final report to AMO and to the CRADA partner.

A draft journal article will be submitted soon for publication.

Conclusions and Outcomes

The MD simulations from this research focused on breakthrough pressure, and evaporation/condensation rates.

The results showed that pore shape can influence the breakthrough pressure, from both through-pore shape variations and cross-sectional pore shape variations. We showed that the impact of cross-sectional pore shape can be simplified into an *effective* pore size, which is proportional to the pore area. This is significant; the membrane literature for several decades has been describing the effect of pore shape on an empirical pore morphology coefficient. This research starts to define this effect in a theoretical way (instead of an empirical value that has been difficult to quantify).

For evaporation and condensation, the steady-state and transient simulations showed that evaporation and condensation rates *at the liquid interface* are equivalent, implying a negligible impact of the membrane structure on the liquid/vapor phase change. These micro-level results confirm our macrolevel understanding of liquid/vapor phase change at interfaces.[1]

However, water vapor diffusion rates in the region far away from the interface during condensation were higher than during evaporation. This implies that diffusion can dominate the transport in these processes, and that any difference between evaporation and condensation could be related to diffusion.

From the results and accumulation of knowledge from this project, we can conclude the following:

- The effect of pore shape on breakthrough pressure trends with pore area, and thus one pore shape does not have an advantage over another in preventing pore breakthrough (equal area means approximately equal vapor transport)

- Because of this, the best pore shape is more related to how to get the most open area (highest porosity) for a given pore area. For example, an optimal structure could be a honeycomb-like structure, which provides a high packing density.

- In general, larger pore sizes lead to higher transport through membrane pores, but also can cause breakthrough of liquid into the pores. Therefore, the ideal pores are just smaller than the pore that will cause breakthrough at the expected max operating pressure. This means that membranes with a very tight pore size distribution (e.g., largest pore is very similar in size to the smallest pore).

- Future research could be used to explore diffusion of vapor through porous membranes of different porosity, tortuosity, and pore size/shape. While there are general models that

1 Note: The effect of very small pores (~10 nm or smaller) will affect evaporation and condensation by changing the equilibrium vapor pressure of the liquid, due to the Kelvin effect (small radii of curvature increase the vapor pressure; this effect causes small water droplets to evaporate more easily than large droplets). This effect was not included in our simulation since there was no pressure forcing the liquid to form a curved meniscus into the membrane pore.

attempt to predict the transport through these membranes, MD simulations could help elucidate the detailed effects of this pore structure, which is especially important given the findings from this research on the importance of diffusion near the liquid/vapor interface.

Implementation:
The results presented in this report can be used to better understand the physics occurring at the membrane/desiccant interface, particularly as it relates to breakthrough pressure and liquid/vapor phase change.

The bullet points in the above *Summary* show how these results can be implemented by the company to (1) better understand how membrane pore structure impacts pore breakthrough pressure, and (2) provide guidance on membrane structures to pursue when selecting or designing a new membrane for these processes.

Future work:
The key future work on diffusion through the membrane was highlighted in the last bullet in the *Summary* above. Another area of potential future research is to investigate further the calculation of water vapor pressure of a desiccant. Many researchers have tried to find a good way to calculate the water vapor pressure of the desiccant, but the only to date have been too specific (i.e., only work for one ion pair), or too inaccurate. We spent some time investigating this, and while our approach could predict the relative vapor pressure of salt solutions for lower concentrations (<10% mass fraction), it overpredicted vapor pressure for higher mass fractions. This task needs more investment, and if successful, this research could have large impact on the development of liquid desiccants for dehumidification.

Experimentally, it would also be valuable to validate the relationship between the pore shape and the breakthrough pressure, and to use experiments to explore condensation and evaporation, including the diffusion near the interface.

Subject Inventions Listing:

None

ROI #:

None

Responsible Technical Contact at Alliance/NREL:

Jason Woods | Jason.Woods@nrel.gov

Name and Email Address of POC at Company:

Peter Luttik | peter.luttik@gmail.com

DOE Program Office:

U.S. Department of Energy Office of Energy Efficiency and Renewable Energy, Advanced Manufacturing Office; funded through a Memorandum Purchase Order (MPO B623397) with Lawrence Livermore National Laboratory.

References:

[1] Purcell, W.R. Interpretation of Capillary Pressure Data. SPE-950369-G. 2(08) (1950) 11-12. https://doi.org/10.2118/950369-G

[2] Cotton, R.A. Membrane filtration : applications, techniques, and problems / edited by Bernard J. Dutka. Pollution engineering and technology ; 17., ed. B.J. Dutka. New York: M. Dekker, 1981.

[3] Kim, B.-S. and P. Harriott. Critical entry pressure for liquids in hydrophobic membranes. Journal of Colloid and Interface Science. 115(1) (1987) 1-8. https://doi.org/10.1016/0021-9797(87)90002-6

[4] Zha, F.F., A.G. Fane, C.J.D. Fell, R.W. Schofield. Critical displacement pressure of a supported liquid membrane. J. Membr. Sci. 75(1) (1992) 69-80. https://doi.org/10.1016/0376-7388(92)80007-7

[5] Servi, A.T., et al. A systematic study of the impact of hydrophobicity on the wetting of MD membranes. J. Membr. Sci. 520 (2016) 850-59. https://doi.org/10.1016/j.memsci.2016.08.021

[6] Rezaei, M., D.M. Warsinger, J.H. Lienhard V, M.C. Duke, T. Matsuura, W.M. Samhaber. Wetting phenomena in membrane distillation: Mechanisms, reversal, and prevention. Water Res. 139 (2018) 329-52. https://doi.org/10.1016/j.watres.2018.03.058

[7] Hereijgers, J., T. Breugelmans, W. De Malsche. Breakthrough in a flat channel membrane microcontactor. Chemical Engineering Research and Design. 94 (2015) 98-104. https://doi.org/10.1016/j.cherd.2014.12.004

[8] Guillen-Burrieza, E., A. Servi, B.S. Lalia, H.A. Arafat. Membrane structure and surface morphology impact on the wetting of MD membranes. J. Membr. Sci. 483 (2015) 94-103. https://doi.org/10.1016/j.memsci.2015.02.024

[9] Woods, J. and E. Kozubal. On the importance of the heat and mass transfer resistances in internally-cooled liquid desiccant dehumidifiers and regenerators. Int. J. Heat Mass Tran. 122 (2018) 324-40. https://doi.org/10.1016/j.ijheatmasstransfer.2018.01.111